ACS Macro Letters

Letter

pubs.acs.org/macroletters

Equilibrium Self-Assembly, Structure, and Dynamics of Clusters of Star-Like Micelles

Vivek M. Prabhu,*[,†] Shrinivas Venkataraman,[‡] Yi Yan Yang,[‡] and James L. Hedrick[§]

[†]Material Measurement Laboratory, National Institute of Standards and Technology, 100 Bureau Drive, Gaithersburg, Maryland 20899, United States

[‡]Institute of Bioengineering and Nanotechnology, 31 Biopolis Way, The Nanos, Singapore 138669, Singapore

[§]IBM Almaden Research Center, 650 Harry Road, San Jose, California 95120, United States

Supporting Information

ABSTRACT: Hierarchical structure and dynamics of clusters of self-assembled star-like micelles formed by oligocarbonate-fluorene end-functionalized poly(ethylene glycol) triblock copolymers were characterized by small-angle neutron scattering and static and dynamic light scattering at concentrations below the gel point. These micelles persist in equilibrium with concentration-dependent sized hierarchical clusters. When probed at length scales within the clusters by dynamic light scattering, the clusters exhibit Zimm dynamics, reminiscent of dilute mesoscale chains. The ability to form chain-like clusters is attributed to the $\pi-\pi$ stacking of the fluorene groups that drives the formation of micelles. This enables a design variable to control the rheology of injectable gels. Further, predictions of the solvent (D_2O) viscosity show deviations consistent with polymers in organic solvents, stressing a need for refinement of molecular theories of polymer dynamics.

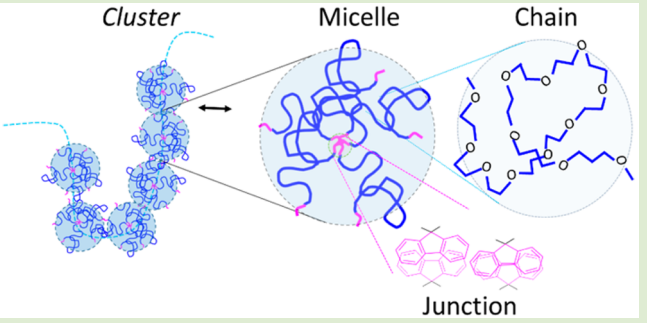

Self-assembled block copolymers are versatile platforms to access functional soft materials for nanobiomedicine, including tissue engineering[1] and drug delivery applications.[2,3] Nanostructured micelles and gels can be designed to spontaneously self-assemble by tailoring parameters including block copolymer concentration, solvent compatibility,[4−6] block molecular mass fraction,[7,8] sequence,[9] and asymmetry.[10,11] Nanostructures may also be encoded in polymers through specific associative interactions, similar to supramolecular polymerization[12] that forms structures through directional and reversible secondary interactions among discrete building units. Soft materials using the principles of block copolymer assembly and supramolecular polymerization offer routes to hierarchically ordered micelles and structured gels.[13−18]

The structure of the solution-dispersed particles or physical gel network should meet the requirements for a desired application. In particular, thermoreversible gels have broad applicability to nanomedicine and may require injectable, spreadable, or mechanically tough platforms. Each niche application may require properties that differ vastly. In this example, injectable thermoreversible gels[19,20] should satisfy at least three criteria: (1) the material must recover its mechanical property after being subjected to a shear force, (2) maintain the microphase separated structure to retain cargo, and (3) have a tailored viscosity and shear modulus. Therefore, one must identify design rules relating the physicochemical parameters with that of macroscopic structure and properties. Enabled by advances in synthetic polymer chemistry, materials can be tailored to suit the broad requirements of functional soft material properties. However, the design rules connecting microscale-to-mesoscale-to-macroscale properties are lacking.

Among synthetic routes to access block copolymers for biomedical applications, aliphatic polycarbonates are a class of biodegradable materials that enable incorporation of a broad range of biocompatible and diverse functional groups to design advanced materials.[2] For example, cholesterol-functionalized polycarbonate-based diblock copolymers were developed that formed nanoscale disk-like micelles.[21] More importantly, the hydrophobic block of these poly(ethylene glycol)-based (PEG) amphiphilic block copolymers could be tailored via copolymerization with trimethylene carbonate (TMC) to encapsulate hydrophobic anticancer drugs.[22] A novel fluorene-functionalized aliphatic polycarbonate (F-TMC) containing PEG amphiphilic block copolymer formed discrete sheets, micellar tapes, and micelles controlled by the relative fraction of F-TMC.[23] Shear-thinning positively charged polycarbonate vitamin E-functionalized PEG triblock copolymers formed spreadable gels with near constant storage modulus, but with antimicrobial properties dependent on the vitamin E block copolymer content.[24] Lastly, injectable, biodegradable gels of a

Received: July 22, 2015
Accepted: September 18, 2015

DOI: 10.1021/acsmacrolett.5b00507
ACS Macro Lett. 2015, 4, 1128−1133

vitamin D-functionalized polycarbonate block copolymer were physically cross-linked by the antibody avastin for in situ-formed hydrogels.[20] In this example, the avastin content and degree of polymerization of vitamin D-functionalized polycarbonate controlled the phase separation and shear modulus. A hierarchical block copolymer micelle structure was hypothesized to control the rheology. However, methods to characterize the hierarchical structure and relationships to rheology were unavailable. In general, the rheological properties, phase stability, and morphology depend on the specific block copolymer chemistry. The hierarchical structures formed by self-assembly of functional block copolymers bear resemblance to supramolecular polymerization systems in the presence of such specific and secondary interactions.

Small-angle neutron scattering (SANS) and static and dynamic light scattering (SLS and DLS, respectively) provide a noninvasive approach to characterize the hierarchical structure from the nanometer to micrometer length scales. SANS was applied to measure the local star-like micelle structure in F-TMC triblock copolymers.[25] Star-like micelles, formed by the association of F-TMC moieties, were the first level of structure below the gel point.

Here, we illustrate the hierarchical structure in an oligocarbonate-fluorene PEG (ABA-F3), Scheme 1, to understand two length scales, above the chain dimension, a basic star-like micelle building block with sticky ends that form larger clusters. The number-average molecular mass of the parent PEG middle block is $M_{n,PEO}$ = 19600 g/mol with two symmetric oligo F-TMC end groups.

Scheme 1. ABA-F3 Triblock Copolymer under Study

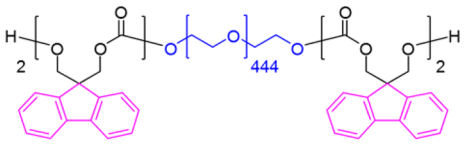

SLS and DLS, at 25 °C, of ABA-F3 in D_2O as a function of concentration (C) used the same samples studied by SANS.[25] The normalized intensity−intensity correlation functions were measured as a function of scattering angle (θ) and analyzed by an a priori approach using a combined single and stretched exponential fit after analysis by inverse-Laplace transform methods confirmed two modes. Figure 1a shows the normalized electric-field time correlation function, $g_1(Q,t)$ (every other angle is shown for clarity). The decay rate Γ_1/Q^2 of the exponential fast-mode plotted versus Q^2 for four concentrations are shown in Figure 1b, where Q is the scattering vector defined by $Q = 4\pi n/\lambda_o \sin \theta/2$, where n is the solvent refractive index and λ_o is the laser wavelength. The translational diffusion constant was determined as $D_1 = \Gamma_1/Q^2$. The hydrodynamic radius (R_H) was quantified by the Stokes−Einstein relation, $R_H = k_BT/6\pi D\eta_s$, with solvent viscosity (η_s), Boltzmann constant (k_B), and temperature (T).

Figure 2 shows the stretched exponential decay rate (Γ_2) results for four concentrations. In this case, Γ_2/Q^2 is not Q-independent, but plateaus at low-Q with systematic deviations at higher Q or smaller probing length scales. As will be illustrated, these deviations represent the internal dynamics of clusters of micelles. The translational diffusion constant of the clusters ($D_2 = \Gamma_2/Q^2$) was estimated from the low-Q plateau and reported as R_H.

The two characteristic R_H values obtained by DLS are shown in Figure 3. The fast-mode R_H is consistent with the micelle size and does not depend on ABA-F3 concentration. The apparent micelle radius of gyration (R_g) determined by SANS is also shown. The micelle size and number of chains per micelle remains weakly dependent on concentration when estimated by a star-like model or SANS Zimm plot.[25] The micelle R_H combined with the R_g from SANS yields an R_g/R_H = 1.2 ± 0.1 when averaged over the four concentrations implying an

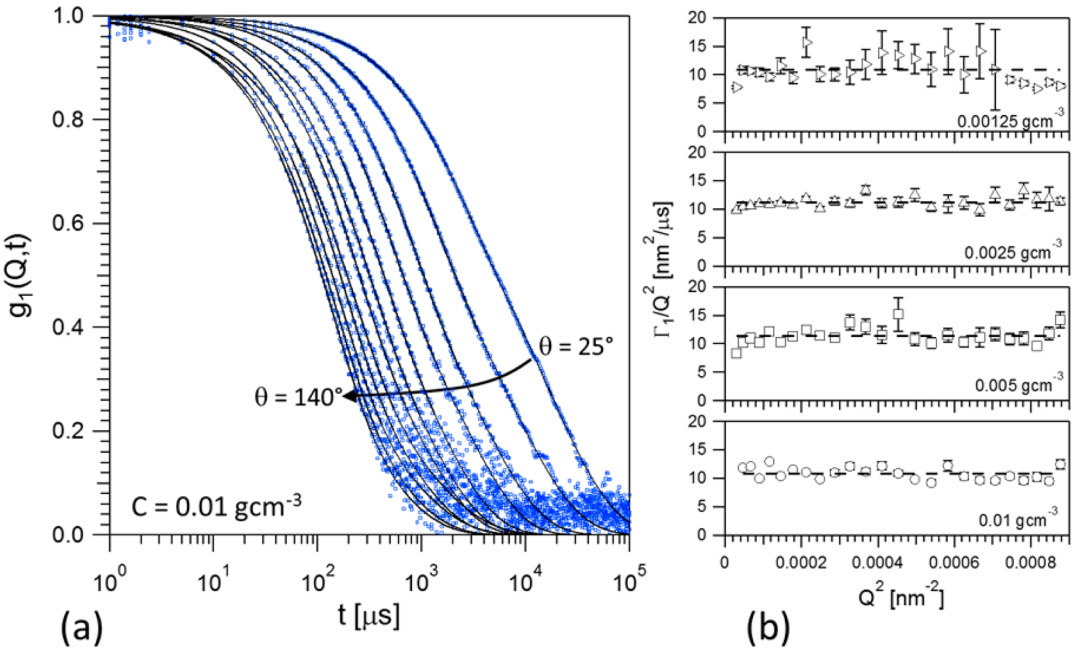

Figure 1. (a) Typical DLS correlation function with fits. (b) Exponential decay rate with Q^2 diffusive scaling for four concentrations of the ABA-F3 polymer in D_2O.

DOI: 10.1021/acsmacrolett.5b00507
ACS Macro Lett. 2015, 4, 1128−1133

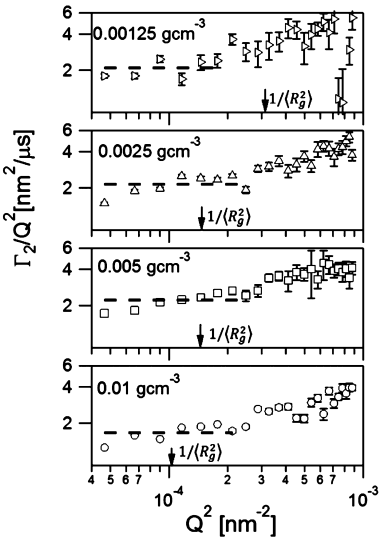

Figure 2. Q^2 normalized decay rate from the stretched exponential fits vs Q^2 on a double-logarithmic plot for ABA-F3 showing diffusive scaling and positive deviations from translational diffusion. The inverse $\langle R^2_g \rangle$ of the cluster is provided.

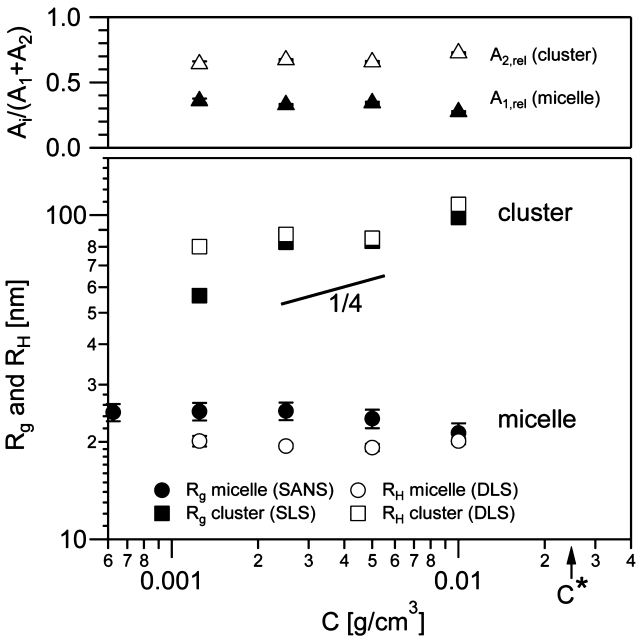

Figure 3. Concentration dependence of the hydrodynamic radius of the cluster and micelles with relative amplitude (upper panel). Apparent radius of gyration by static light scattering (cluster) and small-angle neutron scattering (star-like micelle). The overlap concentration is provided (C^*).

extended structure. This R_g/R_H is compared to calculations[26] for monodisperse Gaussian chains (1.27), regular discs (0.99), uniform spheres (0.77), and measured collapsed polymer chains with hydrophobic stickers[27] ≈ 0.6. A calculation for a 12-arm regular star[28] shows R_g/R_H = 1.17, while more recent simulations find a 10-arm star[29] R_g/R_H = 0.95. A mixture of star and flower-like free micelles cannot be ruled out[30] as it is likely free micelles not associated with a cluster must have the hydrophobic groups buried, as in a flower-like micelle.

The C dependence of the cluster size is shown in Figure 3 below the overlap concentration estimated by the parent PEG polymer ($C^* = 3M_{n,PEG}/4\pi R^3_{g,PEG}N_A \approx 0.024$ g/cm^3) illustrates structure above the micelle and chain dimension ($R_{g,PEG} \approx 7$ nm).[31] In the present case, rather than a solution of disk-like micelles formed from diblock copolymers,[23] a hierarchy was observed based upon star-like micelles with fluorene groups that enable self-assembly with other micelles. The finite-sized clusters in equilibrium with micelles is compared to a $C^{1/4}$ scaling. This scaling is consistent with equilibrium worm-like micelles,[32] where the mean length ~$C^{1/2}$ and by assuming $\langle R_g^2 \rangle$ ~length. While micelles are not observed in aqueous solutions of polyethylene glycol, clustering is known to occur as a function of different end groups with a concentration-dependent correlation length.[33−35] Therefore, the oligo end groups in these telechelic, or triblock copolymers, affects self-assembly and the hierarchical structure. Further insight can be observed by examining the relative amplitudes by DLS.

The relative DLS amplitude, $A_i/(A_1 + A_2)$, of the micelle (i = 1) and cluster slow-mode (i = 2) appears independent of concentration, as shown in Figure 3 for fixed Q = 0.0082 nm^{-1} in the QR_g < 1 limits when sensitive to translational diffusion. The fraction of fast-moving micelles appears constant in dilute solutions as does the micelle size via SANS and DLS. However, since the relative amplitude is insensitive to the concentration, below C^*, we draw an analogy to an equilibrium constant, K = [AB]/[A][B], defined by a reversible reaction such as [A] + [B] ⇄ [AB], a two-state model. Taking the DLS amplitudes as a measure for the fraction of clusters (A_2 ~ [AB] and [B]) and micelles (A_1 ~ [A]), by increasing the concentration of micelle reactant, [A], the ratio of [AB]/[B] would increase in proportion if defined by an equilibrium constant. This appears true above the critical micelle concentration (CMC; 5 × 10^{-5} g/cm^3). This signifies the cluster size may be controlled, but not the relative fraction of micelle to clusters. The cluster formation mechanism may be related to other mesoscale structures,[36] equilibrium supramolecular fibers,[37] worm-like,[32] and multimolecular flower-like[5] micelles, but here the connectivity is driven by the oligocarbonate-fluorene groups. If the F-TMC groups were designed to remain buried in discrete flower-like micelles to eliminate cluster formation until the gel point, one may tailor the rheology and viscosity of the solution. In this spirit, molecular dynamics simulations demonstrate that the flexibility and molecular mass of the middle block control the flower-like to star-like behavior.[38] Lattice theories[39,40] and the framework developed to characterize supramolecular polymerization[12,41] may describe the thermodynamic and kinetic parameters governing our observations.

The scaling properties of the radius of gyration of equilibrium and nonequilibrium polymeric structures have well-known asymptotic scaling laws, such that $\langle R_g^2 \rangle \approx N^{2\nu}l^2$, with degree of polymerization (N) and step length (l).[26] In three dimensions, the scaling exponent, ν, takes on different values, such as for equilibrium clusters with Gaussian statistics, ν = 1/2, and self-avoiding walk, ν = 0.588. In nonequilibrium clusters formed by diffusion-limited aggregation $\nu \approx 0.4$. For objects formed by multifunctional groups, such as polycondensates, $\langle R_g^2 \rangle / l^2 = (f - 1)/2fN$, where f is the functionality of the monomeric species.[28] We estimate the effective cluster degree of polymerization (N_{eff}) by taking the ratio of $\langle R_g^2 \rangle_{cluster}/\langle R_g^2 \rangle_{micelle}$ to understand the concentration dependence of the effective number of micelles per cluster in Figure 4. When estimated by Gaussian, SAW, and nonlinear polycondensate, N_{eff} scales comparable to the mean field $C^{1/2}$

DOI: 10.1021/acsmacrolett.5b00507
ACS Macro Lett. 2015, 4, 1128−1133

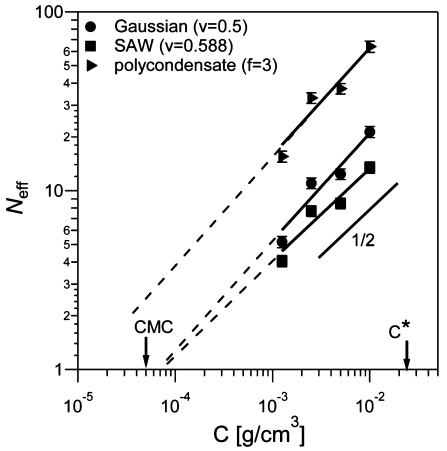

Figure 4. Concentration dependence of the cluster degree of polymerization for linear Gaussian and self-avoiding walk (SAW) and branched polycondensate (f = 3) models. A scaling of 1/2 is shown.

scaling, for reversibly assembling worm-like micelles formed by low molar mass surfactants.[32,42] Using the SLS Zimm plot ($C \rightarrow 0$ limit), the mass-averaged molecular mass (M_w) of 402000 ± 17000 g/mol estimates an ABA-F3 aggregation number of 21 chains. The star-like micelle aggregation number[25] by SANS was 12 at 25 °C, leading to $N_{eff} \approx 1.8$. The linear and branched models extrapolate near this value at the CMC. Therefore, the apparent growth in comparison to the mean field result could result from either linear or branched models, further data are required to better test the effect of branching in the observed clusters. The second virial coefficient by SLS, $-(2.4 \pm 1.4) \times 10^{-5}$ mol·cm^3/g^2, was smaller than solutions of PEG of comparable molecular mass[43] due to the presence of the clustering. The negative, but small, value signifies poor solvent conditions and shows that the clusters are slightly attractive driven by the F-TMC groups.

Returning to the systematic deviations in Figure 2 that occur near the inverse cluster $\langle R^2_g \rangle$, the decay rates above this length scale are linear with Q^3 and displayed as Γ_2/Q^3 in Figure 5a. The stretched exponential β parameter is shown with average β provided in Figure 5b. In the translational diffusion Q-range, β was observed to remains below unity. The stretched exponential $S(Q,t) = S(Q,0)e^{-1.35(\Gamma_Q t)^{2/3}}$ is a limiting form for the dynamic structure factor at the theta condition (screened excluded volume) for the Zimm model,[44] where $\Gamma_Q = (k_BT/6\pi\eta_s)Q^3$ and $\beta = 2/3$. The stretched exponent is comparable to the limiting form for Zimm dynamics, as shown as the solid line in Figure 5b. Fits to Figure 5a provide the quantity $k_BT/6\pi\eta_s$ that estimates the solvent viscosity. This predicted solvent viscosity is greater than, but comparable to, that of D_2O[45] of 0.0011 Pa·s at 25 °C, as shown in Figure 6. These deviations are larger than expected for good versus θ solvent conditions that leads to slightly different decay-rate prefactors.[44]

Rigorous tests for hydrodynamic effects on the dynamics of self-assembling polymers are not available as for linear polymers.[46,47] However, the deviations in the solvent viscosity are consistent with an established literature on local solvent viscosity and relaxation times affected by the presence of polymers in dilute solution, as observed by Lodge.[48] Such observations, made by oscillatory electric birefringence, depolarized Rayleigh scattering, and ^{13}C nuclear magnetic resonance (NMR) find the mean solvent rotational relaxation

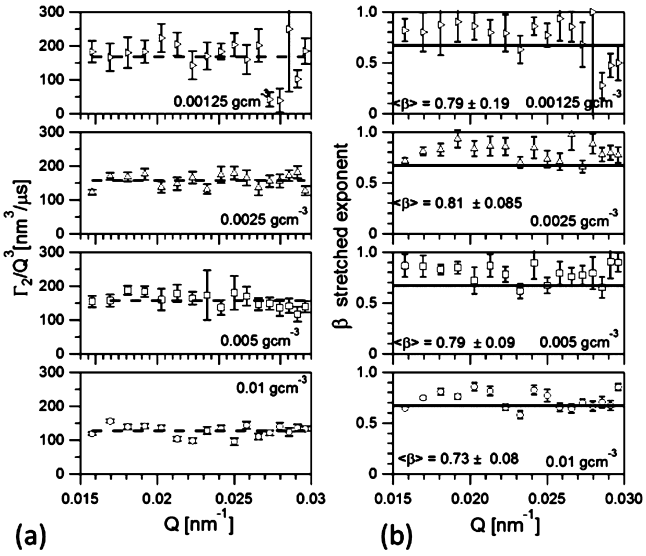

Figure 5. ABA-F3 concentration dependence of the (a) stretched exponential fits to the cluster mode decay rate plotted with Zimm dynamics scaling with fits (dotted line). (b) Stretched exponential parameter (β) with the Zimm limiting value (β = 2/3) as the solid line.

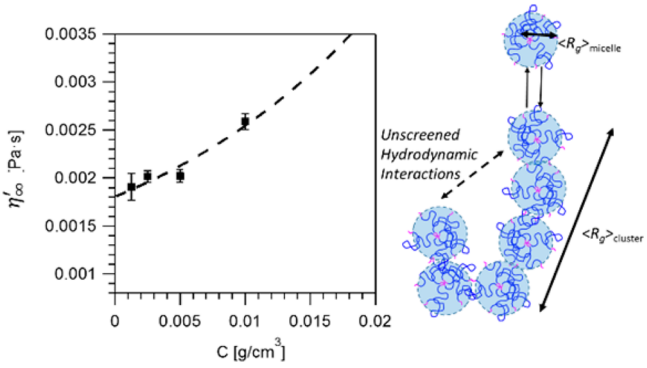

Figure 6. (a) Solvent viscosity from Zimm model with fit to intrinsic effective solvent viscosity model. (b) Schematic of a chain-like cluster of star-like micelles.

times varied systematically with polymer concentration.[48] These high-frequency, molecular-scale origins affect polymer–solvent friction in a manner not considered by continuum medium bead–spring models, where each bead is treated in the Stokes approximation with friction coefficient (ζ) depending on pure solvent viscosity (η_s) and bead radius (a) by $\zeta = 6\pi\eta_s a$. Lodge proposed $\eta'_\infty \cong \eta_s \exp\{C[\eta'_\infty]\}$ to summarize these effects for several polymers in organic solvents. The frequency-independent effective solvent viscosity, η'_∞, is a function of polymer concentration and a local viscosity increment parameter $[\eta'_\infty]$. The sign of $[\eta'_\infty]$ implies local solvent viscosity increases or decreases in the presence of polymer. Both effects are experimentally observed. The dashed line in Figure 6a is a fit to Lodge's expression with an additional baseline term using the extracted solvent viscosity from the Zimm expression (with $\eta_s \rightarrow \eta'_\infty$) that leads to $[\eta'_\infty] = (51 \pm 6)$ cm^3/g and baseline $(7.0 \pm 0.6) \times 10^{-4}$ Pa·s. The magnitude of the $[\eta'_\infty]$ parameter is larger than that observed in organic solvents. Perhaps the effect of polymers on increasing the local viscosity of water may be enhanced by PEG–water hydrogen bonding. The interactions between water and PEG may be characterized by ^{1}H and ^{2}H NMR and perhaps provide further

DOI: 10.1021/acsmacrolett.5b00507
ACS Macro Lett. 2015, 4, 1128–1133

insight.[49] These quiescent Zimm dynamics, in the absence of external flow fields, represent both the flexible chain-like nature of the clusters in equilibrium with micelles in solution. Recent experiments using neutron spin−echo spectroscopy observed an enhanced solvent viscosity in well-defined microgels when analyzed within the Zimm dynamics framework.[50,51]

The hypothesized chain-like structure of micelles, depicted by Figure 6b, must have unscreened hydrodynamic interactions to display Zimm dynamics. The intracluster Zimm dynamics (normal modes of the cluster) were concluded based on two signatures: the scaling of the decay rate, $\Gamma_2(Q)$ with Q^3, and the stretched exponent $\beta \approx 2/3$. Further, the scaling of the cluster radius of gyration and effective degree of polymerization with concentration are consistent with equilibrium worm-like micelles. As C increases and the gel point is crossed, the connectivity of the micelles display a three-dimensional ordering expected by triblock copolymer gels.[52] A crossover to Rouse-like dynamics (screened hydrodynamics, $\beta \approx 1/2$) of the chain-like clusters may not be observed, as collective modes may appear.[53]

The $\pi-\pi$ stacking driven by the hydrophobic oligocarbonate-fluorene groups play the definitive role in the formation of these hierarchical structures as well as at higher molecular mass.[54,55] Given the vast synthetic structures achievable with the polycarbonate chemistries,[56] mesoscale molecular dynamics simulations would enhance the search for novel materials in the spirit of the Materials Genome Initiative.[57] The ability to molecularly connect micelles via hydrophobic linkers supports the hypothesis developed for vitamin D-driven bridging assembly.[20] In the present case, the $\pi-\pi$ stacking interactions appear to induce the hierarchical structure related to the field of supramolecular polymers.[12] A combination of SANS, SLS, and DLS enables quantitative details regarding the structure, phase diagram, and relaxation times that are critical for rheological characterization.

EXPERIMENTAL SECTION

Samples of ABA-F3 were preweighed into 1.5 mL plastic centrifuge tubes and dissolved in aliquots of deuterium oxide (Cambridge Isotopes 99.98 D atom %) to a final concentration of 0.010 g/cm^3. Samples of lower concentration were prepared by successive dilutions with deuterium oxide. All preparation and handling took place in a LabConco Nano-Enclosure Class I BSC with HEPA filtration.

Dynamic and static laser light scattering were performed with a modified Brookhaven BI-200 SM. The 532 nm laser light was from a 2 W Coherent VERDI diode-pumped solid state laser. Glan-Laser polarizer and analyzer (Thorlabs) were used under the vertical polarizer and vertical analyzed condition for all experiments for samples thermostatically controlled to 25 °C using a recirculating bath to control the temperature of the decalin index matching bath. The pinhole just before the photomultiplier tube detector was adjusted for static (1 mm) or dynamic (100 μm) light scattering. The incident laser power was fine-adjusted by neutral density filters.

The static light scattered intensity was corrected for reflection, refraction by standard methods and placed onto the Rayleigh ratio (R_{vv}) intensity scale using toluene with $R_{vv}^{toluene}$ measured by Fytas et al.[55] at 25 °C at 532 nm. A Zimm plot analyzed the static light scattering excess Rayleigh ratio weighted by the DLS amplitude of the cluster,[58,59] such that $I_2(Q) = R_{vv}(Q)A_2/(A_1 + A_2)$ as a function scattering wave vector (Q) and ABA-F3 concentration. At infinite dilution ($C \to 0$) and zero angle ($Q \to 0$), the mass-average molar mass (M_w) is related to $I_2(Q)$ by

$$\frac{HC}{I_2(Q)} = \frac{1}{M_w}\left(1 + \frac{Q^2R_g^2}{3}\right) + 2A_2C + ... \quad (1)$$

where $H = 4\pi n^2(dn/dC)^2/(N_A\lambda_o^4)$ and N_A is Avogadro's number, dn/dC is the refractive index increment, $\langle R_g^2\rangle$ is the mean-square z-average radius of gyration, and A_2 is the second virial coefficient. dn/dC for PEG[43] of 0.133 cm^3/g was applied to the ABA-F3. The concentration-dependent apparent R_g was estimated by the method described by Schmidt et al.[60]

$$R_g^2(C) \equiv 3\frac{d}{dQ^2}\left[\frac{HC}{I_2(Q)}\right]_{C=C_p} \Big/ \left[\frac{HC}{I_2(0)}\right]_{C_p=0} \quad (2)$$

The measured intensity−intensity time correlation function, $G^{(2)}(Q,t)$ is related to the normalized electric-field time correlation function, $g^{(1)}(Q,t)$, by the Siegert relation,

$$G^{(2)}(Q, t) = A(1 + b|g^{(1)}(Q, t)|^2) \quad (3)$$

where A is a baseline $\langle I(Q)\rangle^2$ and b is an instrument spatial coherence factor.[58] The DLS spectrum was fit by eq 4 to quantify the exponential micelle mode and stretched exponential cluster mode contributions.

$$g^{(1)}(Q, t) = A_1e^{-(\Gamma_1(Q)t)} + A_2e^{-(\Gamma_2(Q)t)^\beta} \quad (4)$$

This approach uses a priori information[61] in the form of the presence of micelles from SANS and larger-scale structures by static light scattering. The inverse-Laplace transform methods of CONTIN[62,63] and NNLS[64] (non-negatively constrained least squares) were also carried out using the Brookhaven Instruments software, with both showing two modes. The application of eq 4 agrees quantitatively with translational diffusion coefficient analysis from CONTIN and NNLS and serves to quantify the cluster dynamics at higher scattering angles with respect to a theory.

Uncertainties (error bars) are estimated by one standard deviation of the mean by least-squares minimization of fits to the DLS, SLS, or SANS data. While error bars are shown, they may be smaller than the symbols used in some cases.

ASSOCIATED CONTENT

Supporting Information

The Supporting Information is available free of charge on the ACS Publications website at DOI: 10.1021/acsmacrolett.5b00507.

Sample details, SANS and SLS Zimm plot, CONTIN and NNLS analysis (PDF).

AUTHOR INFORMATION

Corresponding Author

*E-mail: vprabhu@nist.gov.

Notes

The authors declare no competing financial interest.

ACKNOWLEDGMENTS

S.V. and Y.Y.Y. acknowledge funding support from the Institute of Bioengineering and Nanotechnology (Biomedical Research Council, Agency for Science, Technology and Research, Singapore). V.M.P. thanks the support of the NIST Materials Genome Program and Jack Douglas, Guangmin Wei (NIST) and the anonymous reviewers for their critical comments. Certain commercial equipment and materials are identified in this paper in order to specify adequately the experimental procedure. In no case does such identification imply recommendations by the National Institute of Standards and Technology (NIST) nor does it imply that the material or equipment identified is necessarily the best available for this purpose.

DOI: 10.1021/acsmacrolett.5b00507
ACS Macro Lett. 2015, 4, 1128−1133

REFERENCES

(1) Lee, K. Y.; Mooney, D. J. *Chem. Rev.* **2001**, *101* (7), 1869−1879.
(2) Kataoka, K.; Harada, A.; Nagasaki, Y. *Adv. Drug Delivery Rev.* **2001**, *47* (1), 113−131.
(3) Ge, Z.; Liu, S. *Chem. Soc. Rev.* **2013**, *42* (17), 7289−7325.
(4) Honda, C.; Hasegawa, Y.; Hirunuma, R.; Nose, T. *Macromolecules* **1994**, *27* (26), 7660−7668.
(5) Kikuchi, A.; Nose, T. *Macromolecules* **1997**, *30* (4), 896−902.
(6) Fuse, C.; Okabe, S.; Sugihara, S.; Aoshima, S.; Shibayama, M. *Macromolecules* **2004**, *37* (20), 7791−7798.
(7) Mortensen, K.; Brown, W. *Macromolecules* **1993**, *26* (16), 4128−4135.
(8) Lin, S.; Lin, J.; Nose, T.; Iyoda, T. *J. Polym. Sci., Part B: Polym. Phys.* **2007**, *45* (11), 1333−1343.
(9) Hong, L.; Zhu, F.; Li, J.; Ngai, T.; Xie, Z.; Wu, C. *Macromolecules* **2008**, *41* (6), 2219−2227.
(10) Mai, Y.; Eisenberg, A. *Chem. Soc. Rev.* **2012**, *41* (18), 5969−5985.
(11) Gröschel, A. H.; Schacher, F. H.; Schmalz, H.; Borisov, O. V.; Zhulina, E. B.; Walther, A.; Müller, A. H. E. *Nat. Commun.* **2012**, *3*, 710.
(12) De Greef, T. F. A.; Smulders, M. M. J.; Wolffs, M.; Schenning, A. P. H. J.; Sijbesma, R. P.; Meijer, E. W. *Chem. Rev.* **2009**, *109* (11), 5687−5754.
(13) Wang, X.; Guerin, G.; Wang, H.; Wang, Y.; Manners, I.; Winnik, M. A. *Science* **2007**, *317* (5838), 644−647.
(14) Feldman, K. E.; Kade, M. J.; de Greef, T. F. A.; Meijer, E. W.; Kramer, E. J.; Hawker, C. J. *Macromolecules* **2008**, *41* (13), 4694−4700.
(15) Olsen, B. D.; Kornfield, J. A.; Tirrell, D. A. *Macromolecules* **2010**, *43* (21), 9094−9099.
(16) Wang, Q.; Mynar, J. L.; Yoshida, M.; Lee, E.; Lee, M.; Okuro, K.; Kinbara, K.; Aida, T. *Nature* **2010**, *463* (7279), 339−343.
(17) Zhang, K.; Aiba, M.; Fahs, G. B.; Hudson, A. G.; Chiang, W. D.; Moore, R. B.; Ueda, M.; Long, T. E. *Polym. Chem.* **2015**, *6* (13), 2434−2444.
(18) Görl, D.; Zhang, X.; Stepanenko, V.; Würthner, F. *Nat. Commun.* **2015**, *6*, 7009.
(19) Yu, L.; Ding, J. *Chem. Soc. Rev.* **2008**, *37* (8), 1473−1481.
(20) Lee, A. L. Z.; Ng, V. W. L.; Gao, S.; Hedrick, J. L.; Yang, Y. Y. *Biomacromolecules* **2015**, *16* (2), 465−475.
(21) Venkataraman, S.; Lee, A. L.; Maune, H. T.; Hedrick, J. L.; Prabhu, V. M.; Yang, Y. Y. *Macromolecules* **2013**, *46* (12), 4839−4846.
(22) Ke, X.; Ng, V. W. L.; Ono, R. J.; Chan, J. M. W.; Krishnamurthy, S.; Wang, Y.; Hedrick, J. L.; Yang, Y. Y. *J. Controlled Release* **2014**, *193*, 9−26.
(23) Venkataraman, S.; Hedrick, J. L.; Yang, Y. Y. *Polym. Chem.* **2014**, *5* (6), 2035−2040.
(24) Lee, A. L. Z.; Ng, V. W. L.; Wang, W.; Hedrick, J. L.; Yang, Y. Y. *Biomaterials* **2013**, *34* (38), 10278−10286.
(25) Prabhu, V. M.; Venkataraman, S.; Yang, Y. Y.; Hedrick, J. L. *Macromol. Symp.* **2015**, Accepted for publication.
(26) Mansfield, M. L.; Douglas, J. F. *J. Chem. Phys.* **2013**, *139* (4), 044901.
(27) Zhang, G. Z.; Winnik, F. M.; Wu, C. *Phys. Rev. Lett.* **2003**, *90* (3), 035506.
(28) Burchard, W. *Adv. Polym. Sci.* **1983**, *48*, 1−124.
(29) Singh, S. P.; Huang, C.-C.; Westphal, E.; Gompper, G.; Winkler, R. G. *J. Chem. Phys.* **2014**, *141* (8), 084901.
(30) Weiss, J.; Wienk, H.; Boelens, R.; Laschewsky, A. *Macromol. Chem. Phys.* **2014**, *215* (9), 915−919.
(31) Devanand, K.; Selser, J. C. *Macromolecules* **1991**, *24* (22), 5943−5947.
(32) Cates, M.; Candau, S. *J. Phys.: Condens. Matter* **1990**, *2* (33), 6869−6892.
(33) Hammouda, B.; Ho, D.; Kline, S. *Macromolecules* **2002**, *35* (22), 8578−8585.
(34) Hammouda, B.; Ho, D. L. *J. Polym. Sci., Part B: Polym. Phys.* **2007**, *45* (16), 2196−2200.
(35) Hammouda, B. *J. Chem. Phys.* **2010**, *133* (8), 084901.
(36) Versteegen, R. M.; van Beek, D. J. M.; Sijbesma, R. P.; Vlassopoulos, D.; Fytas, G.; Meijer, E. W. *J. Am. Chem. Soc.* **2005**, *127* (40), 13862−13868.
(37) Albertazzi, L.; van der Zwaag, D.; Leenders, C. M. A.; Fitzner, R.; van der Hofstad, R. W.; Meijer, E. W. *Science* **2014**, *344* (6183), 491−495.
(38) Khalatur, P. G.; Khokhlov, A. R.; Kovalenko, J. N.; Mologin, D. A. *J. Chem. Phys.* **1999**, *110* (12), 6039−6049.
(39) Tanaka, F. *Macromolecules* **1989**, *22* (4), 1988−1994.
(40) Dudowicz, J.; Freed, K. F.; Douglas, J. F. *J. Chem. Phys.* **2012**, *136* (6), 064903.
(41) Smulders, M. M. J.; Nieuwenhuizen, M. M. L.; de Greef, T. F. A.; van der Schoot, P.; Schenning, A. P. H. J.; Meijer, E. W. *Chem. - Eur. J.* **2010**, *16* (1), 362−367.
(42) Dreiss, C. A. *Soft Matter* **2007**, *3* (8), 956−970.
(43) Venohr, H.; Fischer, V.; Strunk, H.; Borchard, W. *Eur. Polym. J.* **1998**, *34* (5−6), 723−732.
(44) Doi, M.; Edwards, S. F. *The Theory of Polymer Dynamics*; Oxford University Press: New York, 1995.
(45) Hardy, R.; Cottington, R. *J. Res. Natl. Bur. Stand.* **1949**, *42* (6), 573−578.
(46) Han, C.; Akcasu, A. *Macromolecules* **1981**, *14* (4), 1080−1084.
(47) Dai, Z.; Ngai, T.; Wu, C. *Soft Matter* **2011**, *7* (9), 4111−4121.
(48) Lodge, T. *J. Phys. Chem.* **1993**, *97* (8), 1480−1487.
(49) Lusse, S.; Arnold, K. *Macromolecules* **1996**, *29* (12), 4251−4257.
(50) Scherzinger, C.; Holderer, O.; Richter, D.; Richtering, W. *Phys. Chem. Chem. Phys.* **2012**, *14* (8), 2762−2768.
(51) Maccarrone, S.; Scherzinger, C.; Holderer, O.; Lindner, P.; Sharp, M.; Richtering, W.; Richter, D. *Macromolecules* **2014**, *47* (17), 5982−5988.
(52) Mortensen, K. *J. Phys.: Condens. Matter* **1996**, *8* (25A), A103−A124.
(53) Hiroi, T.; Ohl, M.; Sakai, T.; Shibayama, M. *Macromolecules* **2014**, *47* (2), 763−770.
(54) Fytas, G.; Nothofer, H. G.; Scherf, U.; Vlassopoulos, D.; Meier, G. *Macromolecules* **2002**, *35* (2), 481−488.
(55) Somma, E.; Loppinet, B.; Chi, C.; Fytas, G.; Wegner, G. *Phys. Chem. Chem. Phys.* **2006**, *8* (23), 2773−2778.
(56) Engler, A. C.; Ke, X.; Gao, S.; Chan, J. M. W.; Coady, D. J.; Ono, R. J.; Lubbers, R.; Nelson, A.; Yang, Y. Y.; Hedrick, J. L. *Macromolecules* **2015**, *48* (6), 1673−1678.
(57) de Pablo, J. J.; Jones, B.; Lind, C.; Ozolins, V.; Ramirez, A. P. *Curr. Opin. Solid State Mater. Sci.* **2014**, *18* (2), 99−117.
(58) Fytas, G. *Scattering: Scattering and Inverse Scattering in Pure and Applied Science*; Academic Press: San Diego, CA, 2003; Vol. *35*, pp 849−863.
(59) Sedlak, M. *J. Phys. Chem. B* **2006**, *110* (9), 4329−4338.
(60) Beer, M.; Schmidt, M.; Muthukumar, M. *Macromolecules* **1997**, *30* (26), 8375−8385.
(61) Pike, E. R. In *Scattering Techniques Applied to Supramolecular and Nonequilibrium Systems*; Chen, S-H, Chu, B., Nossal, R., Eds.; Plenum Press: New York, 1981; pp 179−199.
(62) Provencher, S. *Comput. Phys. Commun.* **1982**, *27* (3), 213−227.
(63) Provencher, S. *Comput. Phys. Commun.* **1982**, *27* (3), 229−242.
(64) Grabowski, E.; Morrison, I. In *Measurements of Suspended Particles by Quasi-Elastic Light Scattering*; Dahneke, B., Ed.; Wiley-Interscience: New York, 1983; Chapter 7, pp 199−236.

DOI: 10.1021/acsmacrolett.5b00507
ACS Macro Lett. 2015, 4, 1128−1133